Journal of Power Sources 242 (2013) 70–77

Contents lists available at SciVerse ScienceDirect

Journal of Power Sources

journal homepage: www.elsevier.com/locate/jpowsour

A study of the effect of water management and electrode flooding on the dimensional change of polymer electrolyte fuel cells

Thomas J. Mason, Jason Millichamp, Tobias P. Neville, Paul R. Shearing, Stefaan Simons, Daniel J.L. Brett*

Electrochemical Innovation Lab, Department of Chemical Engineering, UCL, London WC1E 7JE, UK[1]

HIGHLIGHTS

- Direct correlation between membrane thickness and conductivity.
- Initial hydration of membrane leads to significant swelling of MEA.
- Dynamic electro-mechanical analysis on operational MEAs during flooding demonstrated.
- Flooding leads to a significant change in membrane conductivity and thickness change.

GRAPHICAL ABSTRACT

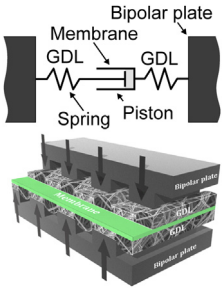

ARTICLE INFO

Article history:
Received 28 August 2012
Received in revised form
24 February 2013
Accepted 9 May 2013
Available online 21 May 2013

Keywords:
Water management
Diagnostics
Flooding
Electrochemical impedance spectroscopy
Swelling
Compression

ABSTRACT

Water management and flooding play an important role in the performance and durability of polymer electrolyte fuel cells (PEFCs). In this study, a dynamic electro-mechanical analysis is performed to examine the performance of a working PEFC during hydration transients and flooding events. Cell resistance is measured using electrochemical impedance spectroscopy (EIS), and the stress/strain characteristics – cell compression and membrane electrode assembly (MEA) dimensional change – are studied using a controlled compression unit (CCU).

Ex-situ measurements of membrane thickness as a function of hydration level provide a direct correlation between ionic conductivity and thickness. During initial hydration of Nafion membranes there is a direct relationship between membrane conductivity and dimensional change (swelling) of MEAs. Electrode flooding is found to result in membrane hydration and an increase in stress or strain, depending on the compression mode of the fuel cell. Results suggest that hydration cycles and flooding events can lead to cell degradation due to the stresses imposed.

1. Introduction

Polymer electrolyte fuel cells (PEFCs) have a major role to play in the transition from a carbon intensive economy to a sustainable low carbon future. Intensive research and development in this area has focused on key issues such as catalyst development, low cost materials, performance and durability. A large section of research in the area of performance degradation has focused on water management, an area that has been extensively reviewed [1–3].

Water management inside a PEFC is a function of generation (reaction), various transport processes and the effect on the proton conductivity of the membrane. It has a significant impact on PEFC performance and is one of the major challenges facing the development of this technology [4]. Mechanisms of particular importance include electro-osmotic drag, associated with the migration of protons, which draws water from the anode through

* Corresponding author. Tel.: +44 (0)20 7679 3310.
E-mail address: d.brett@ucl.ac.uk (D.J.L. Brett).
[1] Web: www.ucl.ac.uk/centre-for-co2-technology.

0378-7753/$ – see front matter © 2013 Elsevier B.V. All rights reserved.
http://dx.doi.org/10.1016/j.jpowsour.2013.05.045

the electrolyte to the cathode [5]; back diffusion of water from the cathode to the anode due to hydraulic pressure difference; hydration of the membrane which effects the conductivity of the electrolyte [6] and the fact that water is produced at the cathode catalyst layer (CCL) by the oxygen reduction reaction. Accumulation of water limits the performance of the PEFC due to mass transport limitation of flooded electrodes [7]. Effective water management requires careful consideration of fuel cell component design, the materials used and the operating conditions imposed.

When water builds up at the cathode CCL, the mechanisms for removing it include the hydrophobic nature of the elements of the gas diffusion layer (GDL), the operating temperature of the fuel cell (removal as water vapour), and back diffusion through the electrolyte. When the rate of water accumulation at the CCL exceeds the removal rate, the pores in the GDL, and ultimately the flow channel, get blocked (flooding). When this occurs the catalyst is effectively starved of reactant and hence the performance of the cell decreases.

Extensive research has taken place into understanding water management and developing new materials and cell designs to mitigate flooding; this includes examining the effects of GDL material [8,9], PTFE content [10,11], micro-porous layers (MPL) [12,13], porosity of the GDL/MPL structure [14,15], flow field design [16,17], CCL materials and microstructure [18,19] and fuel cell operating conditions [20–22]. The GDL is a particularly important component for water management; an understanding on the various chemical and physical properties of which is particularly important for effective MEA design [23].

In order to study fuel cells and obtain a better understanding of their internal workings, a range of diagnostics have been developed [24]; of these, several key techniques have been used to analyse *in-situ* effects of water management and flooding. An electrochemical impedance spectroscopy (EIS) technique was used by Canut*et al.* to study membrane conductivity during drying and flooding [25]. Barbir *et al.* showed, again using EIS, a relationship between cell resistance and humidification level with pressure drop analysis used concurrently to show the onset of water flooding [26]. Membrane conductivity spatial mapping has been demonstrated by Brett *et al.* [27] and applied by Hakenjos *et al.* in conjunction with temperature distribution analysis to examine water flooding [28].

Experimental diagnostics of water management and in particular water flooding have been extensively researched with particular focus on imaging techniques such as optical visualisation [22,29–31], X-ray imaging [32,33], neutron imaging [34–36] and magnetic resonance imaging [37,38].

The diagnostic techniques applied to the study of water management and flooding have tended to concentrate on the effect of membrane conductivity and the mass transport limiting effect of water in the GDL and electrode. Extensive work has been dedicated to the understanding of Nafion in order to characterise the structure and distribution of water [39]; however, little has been done to examine the effect of dimensional change associated with changes in the hydration of the membrane and its impact on cell and stack performance. This paper applies a new technique to investigate the effects of water flooding on operating PEFCs by looking at the resistance of the membrane and its thickness change in real time.

2. Experimental

Fuel cell operation was carried out using a commercially available cell compression unit (CCU) (Pragma Industries SAS, France), which allows controlled compression (resolution of 0.01 MPa) or displacement of the fuel cell with simultaneous relative real time displacement measurement (resolution of 1 μm). The CCU features a 'floating piston' style fuel cell (Fig. 1) that allows compression to be applied evenly onto the active area of the fuel cell to allow

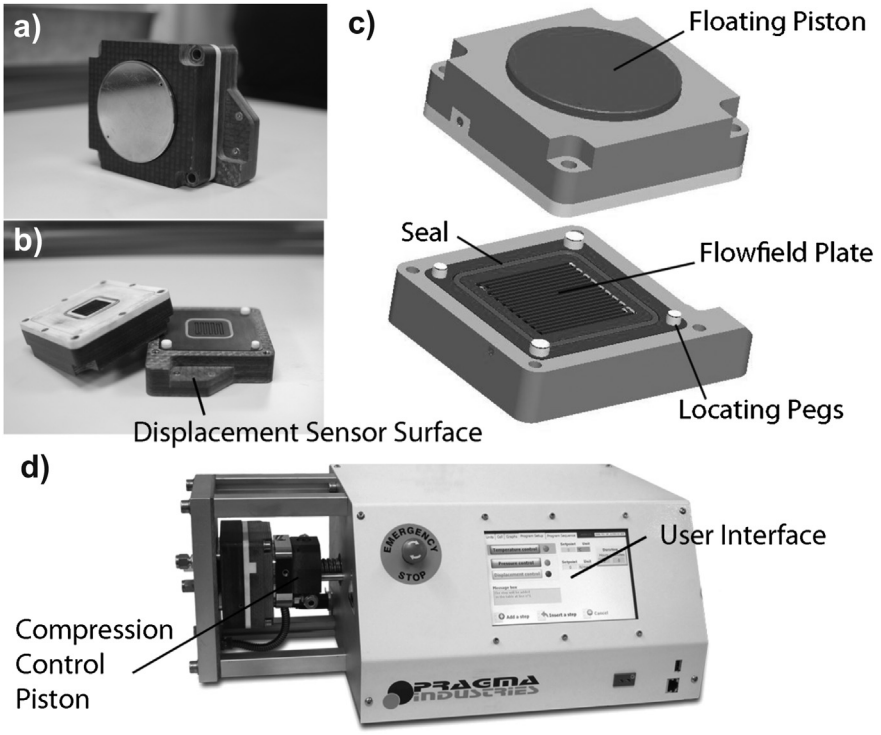

Fig. 1. Cell compression unit (CCU) with floating piston fuel cell. (a–c) show the floating piston cell with the single serpentine flow field design and gas seals, with the displacement sensor surface located on the static anode side of the cell. (d) shows the CCU with the cell loaded with the compression control piston acting on the 'floating' cathode flow field. (Images (c) and (d) courtesy of Pragma Industries SAS, France).

accurate measurement of the real compression applied to the cell. The fuel cell used has an active area of 5 cm^2 using a single serpentine flow field design with land and channel width of 1.2 mm and 1.1 mm respectively. Temperature control, with an accuracy of <1 °C, was achieved with the CCU and all testing done at a fuel cell operating temperature of 80 °C. The measured effective thermal expansion coefficient of the CCU was determined to be 1.92 μm $°C^{-1}$, with the CCU being to maintain temperature to within ±0.2 °C, meaning displacement variation during experiments due to temperature fluctuations is minimal (<1 μm).When the CCU was operated in constant compression mode a setting of 0.2 MPa was used, this is the minimum compression for which no gas leaks occur. The complete system layout is depicted in Fig. 2.

Electrochemical control of the system was achieved with an Iviumstat. XRipotentiostat (Alvatek Ltd, UK) with the resistance measurements carried out using EIS at a set frequency of 5 kHz and amplitude of 15 mV. This frequency was chosen after running a full impedance frequency sweep with the frequency closest to the high frequency intercept being chosen.

Humidification of the gas streams was achieved using an in-housedeveloped system which was calibrated using a heated probe humidity sensor (Vaisala HMT337, Sweden) and was operated at 100% RH at between 80 and 85 °C depending on the particular experiment. Gas flow was kept constant for all operating fuel cell experiments at either 50 or 100 ml min^{-1} (calibrated mass flow controller: EL-FLOW, Bronkhorst, UK) for hydrogen, nitrogen and air at the anode and cathode respectively (all gasses Zero Grade, BOC UK).

The membrane electrode assemblies (MEAs)used in this work were produced in-house using Nafion 117 electrolyte (Fuel Cell Store, US) and Alfa Aesar electrodes (045372, Alfa Aesar, UK) with an active area of 5 cm^2. The MEAs were pressed (Carver 4122CE, US) at 170 °C for 4 min with a pressure applied of 450 PSI. The cells were stored at room temperature and humidity prior to pre-conditioning before each experiment. Pre-conditioning of the fuel cells was carried out by flowing 100% RH nitrogen and air over the anode and cathode respectively at a flow rate of 50 ml min^{-1} each for 30 min followed by 100% RH hydrogen and air at 100 ml min^{-1} for 30 min at 100 mA cm^{-2}. For the start-up experiments the MEAs were placed in a drying oven for 1 h at 110 °C to ensure that the MEA were in a notionally 'dry state' and minimizing the water content of the electrolyte.

The CCU can operate in two different modes to enable control and observation of the displacement and compression of the fuel cell. When control of the compression is desired the displacement is measured and vice versa, an expanding component is associated with a negative displacement response and an increasing force exerted by an expanding component as a positive pressure change.

The different operating modes are depicted in Fig. 3 using the analogy of a spring and piston for the GDL and electrolyte respectively. In controlled displacement mode, Fig. 3(b), as the electrolyte hydrates (piston expands) the springs (GDLs) are compressed (crushed). In controlled compression mode, Fig. 3(c), the piston expands and the thickness of the MEA increases, allowing the compression of the springs (GDLs) to remain constant.

Ex-situ Nafion water content experiments were carried out by measuring the thickness at three random points on the membrane using a micrometer, then taking an average. Weight measurements were taken using an analytical balance (Sartorius MC1 Analytic AC 210 P, US) with the water content controlled by immersing the samples in de-ionized water at 80 °C for 1 h, then removing and measuring the thickness and weight every 2 min to build up the dataset as the sample dries. This process was repeated multiple times to build up the data set. Data for low water content were taken after >1 h of storage in a drying oven at 110 °C.

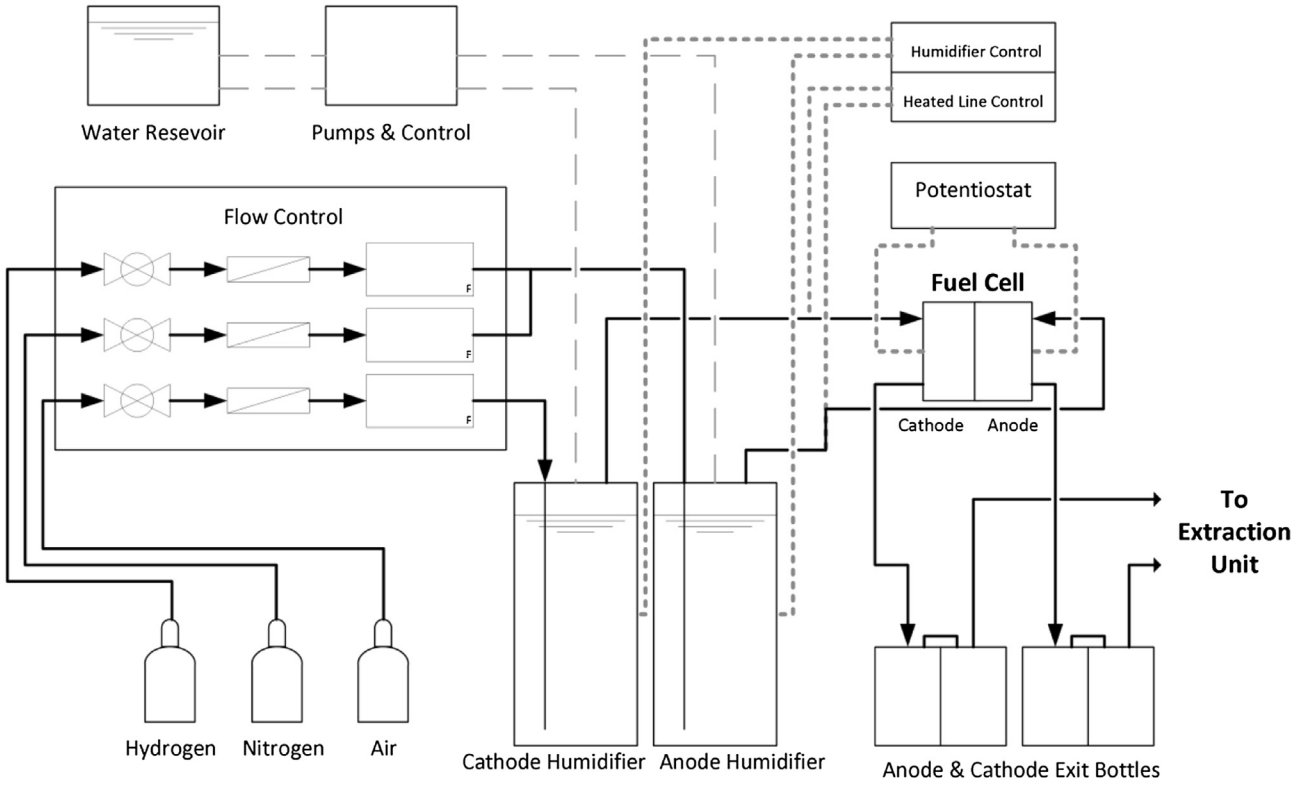

Fig. 2. Piping and instrumentation diagram for fuel cell testing set up.

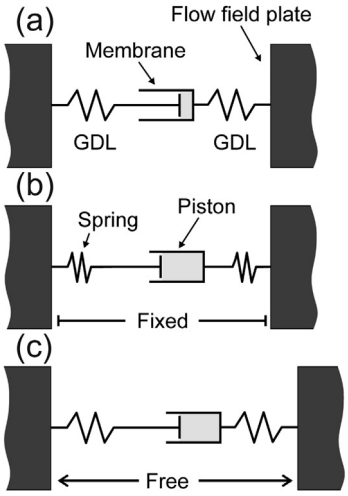

Fig. 3. Illustration showing the analogy between the MEA components and spring/piston mechanical connection. (a) MEA system within two flow field plates and the GDL and electrolyte shown as a spring and piston respectively; (b) Electrolyte membrane swelling in controlled displacement mode, the piston expands the springs are compressed; (c) controlled compression mode, the electrolyte expands and the compression remains constant leading to displacement of the flow field plates and no compression of the springs (GDLs).

3. Results and discussion

From electrochemical impedance spectroscopy measurements, Fig. 4 shows a Nyquist plot for the fuel cell operated at 0.8 V. The high frequency intercept with the real axis represents the Ohmic resistance of the system, which is primarily due to the electrolyte membrane. A frequency of 5 kHz was used to monitor the resistance with time, measurements made every 1 s to follow transients.

3.1. Individual membrane and GDL properties

Before studying the effect of compression, dimensional change and water management on whole MEAs, it is necessary to characterise the individual components, i.e. the membrane and GDL.

Membrane Electrolyte: The relationship between water content and thickness of Nafion 117 (pure membrane, no GDL) is described by Fig. 5. Measurements were taken by weighing the sample and measuring the thickness with a micrometre. The water content of the electrolyte, λ (mol H_2O/mol SO_3^-), is related to the mass of the sample by Eq. (1) [40].

$$\lambda\left(\frac{\text{mol } H_2O}{\text{mol } H_2O}\right) = \frac{(M_{Test} - M_{Dry}) \bullet \dfrac{1 \text{ mole } H_2O}{18.015 \text{ g } H_2O}}{M_{Dry} \bullet \dfrac{1 \text{ mole } SO_3^-}{1100 \text{ g Membrane}}} \quad (1)$$

Under ambient lab conditions the Nafion 117 material used has a measured thickness of 178 ± 2 μm, this is in agreement with the '117' assignment (7 mils = 177.8 μm). Each thickness measurement was taken three times at various positions on the Nafion samples, giving rise to the error bars shown. The relationship between thickness and water content shows a linear fit with a gradient of 0.49 λ μm^{-1}.

The dashed lines represent three water content regimes: $\lambda = 0$ represents a dry membrane; $0 < \lambda < 16.8$ represents the water content in equilibrium with air, and $16.8 < \lambda < 22$ for the membrane in equilibrium with liquid water [7].

Fig. 5 shows a linear relationship between water content and thickness over the 'vapour' range. Upon exposure to liquid water, there is a sharp increase in the water content corresponding to liquid water saturation; this result suggests that exposure of an operating membrane to significant amounts of liquid water, as might be experienced during a flooding event, could lead to a relatively large increase in thickness.

Springer *et al.* [7], presented a relationship between the membrane conductivity (S cm^{-1}) of Nafion 117 and its water content (λ). It is therefore possible to transform the water content vs. thickness trend shown in Fig. 5 into a relationship between thickness and conductivity (and therefore resistance), Eq. (2) shows the derived relationship for membrane conductivity (at 30 °C) with absolute thickness (t).

$$\sigma(\text{S cm}^{-1}) = 25.181 \times t(\text{cm}) - 0.4313 \quad (2)$$

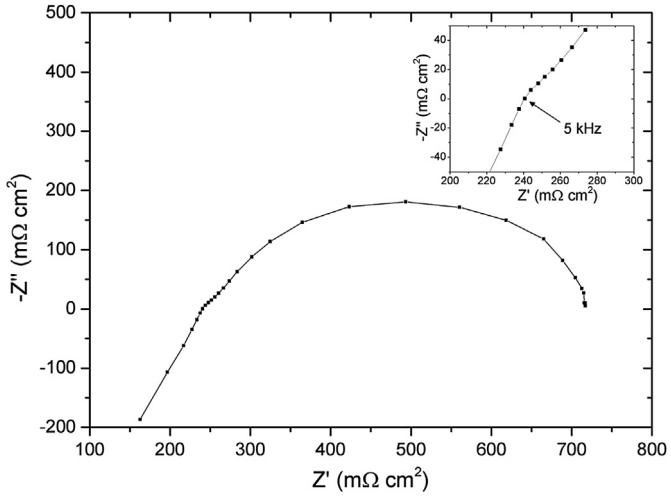

Fig. 4. Nyquist plot of the fuel cell operating at 0.8 V with a voltage amplitude of 15 mV and a frequency range of 10 kHz to 0.1 Hz. Figure inset shows the 5 kHz point where the impedance is taken during the time scans.

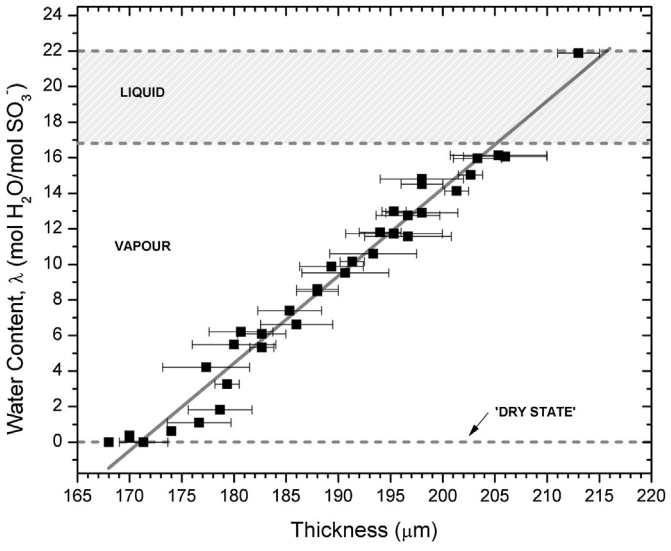

Fig. 5. Relationship between thickness and water content of Nafion 117 across a range of hydration levels. Dry conditions were generated by treatment at 110 °C for 1 h, vapour equilibrated measurements we taken under lab conditions and fully hydrated conditions generated by immersion in liquid water at 80 °C. Water content was calculated using Eq. (1), the linear fit shown has a gradient of 0.49 λ μm^{-1}. The dashed lines represent three key water contents: dry, vapour and liquid.

In this study, the derived relationship will be referred to as '*ex-situ*' membrane, whereas the response obtained from the CCU experimentation of whole MEAs is referred to as the 'startup' result.

Gas diffusion layer: When a fuel cell is operated in constant displacement mode, which is analogous to a fuel cell compressed by tie-rods without stress relief, the compression changes as the membrane swells. This swelling of the membrane will impose a force on the GDL material. Previous work has shown that there is a direct relationship between the compression force applied to a GDL, its change in thickness and the resulting resistance of the sample, this being a combination of a change in the effective resistance of the GDL (as the fibres coalesce under compression) and the contact resistance with the flow field plate [41]. Fig. 6 shows the relationship between resistance and compression for the GDL used to make the MEAs (Toray H060), in the same CCU apparatus. The gradient of the trend is -9.2 mΩ cm^2 MPa^{-1}, this agrees well with the work previously published where a value of ca. -10 mΩ cm^2 MPa^{-1} was obtained for this region of compression [41].

Variation of water vapour content or the introduction of liquid water to GDL-only samples showed no significant change in sample thickness. Changes in MEA sample dimensions are therefore attributed exclusively to the membrane.

3.2. Fuel cell start-up

Upon start-up of a fuel cell, the membrane must be hydrated from a 'dry state' to operational conditions; typically this is achieved by passing a humidified gas through the flow field; this process involves the membrane physically expanding (swelling) which has an impact on the adjacent GDL. Fig. 7(a) shows the resistance and displacement trend in controlled compression mode for the fuel cell with humidified nitrogen flowing on one side of the cell (80 °C, N_2 flow rate of 100 ml min^{-1} at 100% RH). There is a correlation between the resistance and thickness change, both reaching equilibrium after ~125 s. Fig. 7(b) shows the hydration transition under the same conditions in constrained mode (controlled displacement mode); when the MEA is hydrated, resistance decreases and the pressure exerted on the MEA increases significantly. Water content is dominant over sample thickness in deciding the ionic resistance of the membrane. As such, when the membrane swells a resistance decrease is expected despite the increase in thickness. The transition to equilibrium occurring over a similar, but shorter, time period than that in constant pressure mode.

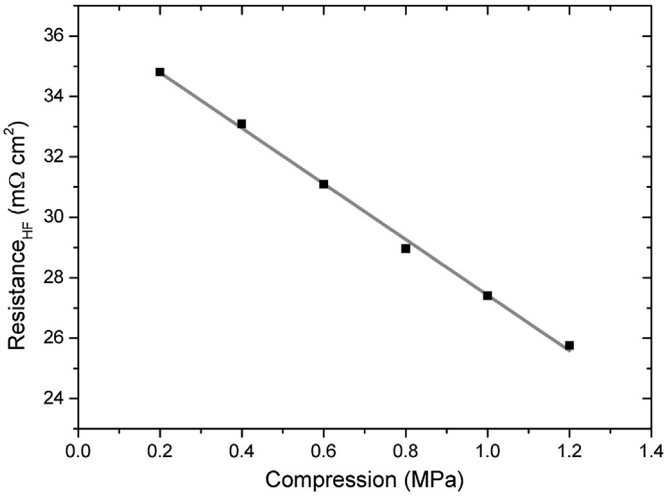

Fig. 6. Relationship between resistance and compression of a single piece of Toray H060 measured using the CCU. The gradient of the line is -9.2 mΩ cm^2 MPa^{-1}. In-between each step increase in compression the sample was returned to 0.2 MPa.

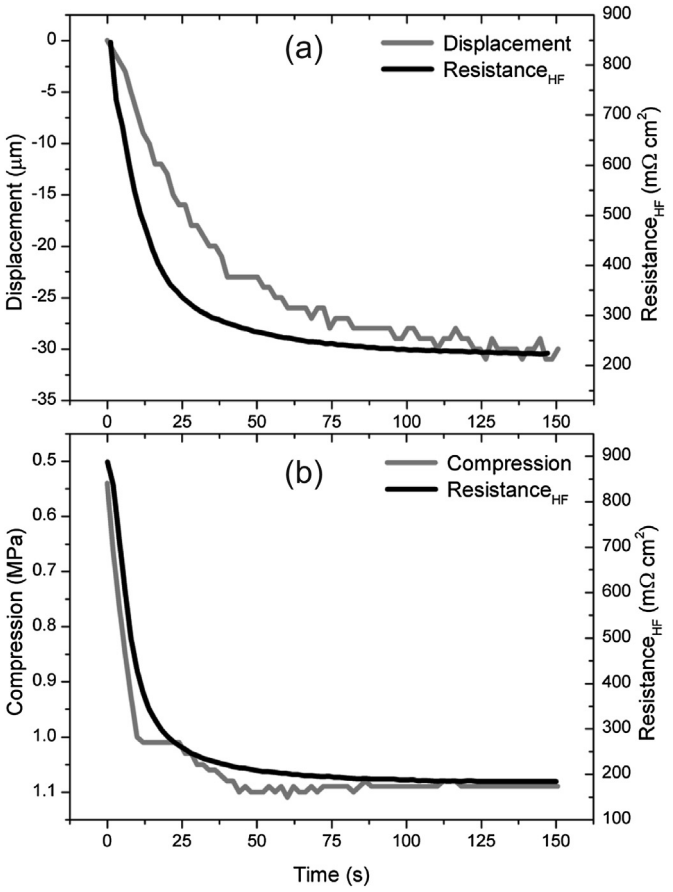

Fig. 7. (a) Controlled compression mode (0.2 MPa): The displacement and high frequency resistance response for hydration of the fuel cell from a dry state with humidified nitrogen. (b) Controlled displacement mode: Initial hydration of an MEA with constrained displacement to enable measurement of compression change during start-up. Operating conditions for both tests were cell temperature at 80 °C and 100% RH on the anode with the cathode sealed. The gas flow rate was 100 ml min^{-1}.

Some variability in the conductivity of notionally dry MEAs was observed between different samples. However, the final resistance was always of the order of 200 mΩ cm^2. In controlled compression mode the expansion of the membrane leads to an increase in the membrane thickness (swelling) of 30 μm coupled to a reduction in resistance of ~630 mΩ cm^2. However, constrained compression mode does not best reproduce the most common method of fuel cell construction (tie-bars), which is better replicated by the constrained displacement operating mode. In controlled displacement operating mode the compression change upon start-up (hydration) is +0.56 MPa. The final equilibrium MEA resistance is 22% lower for constrained mode, this is expected due to the improved contact resistance from the crushing of the GDL materials with increased compression (see Fig. 6).

For a fuel cell system free to expand, these small cell level changes can become quite significant. For example, a 60-cell stack would expand by ~1.8 mm if each cell were to undergo the change associates with hydration as shown in Fig. 7(a). For a physically constrained system (i.e. tie rods without stress relief), significant change in internal compression force will occur each time a fuel cell MEA undergoes a hydration cycle, which will often be a feature of a standard start-up/shutdown cycle. The stresses imposed will be amplified by the number of cells in a stack. Without an external

means of relieving stress, the GDL, as the most mechanically compliant component in the stack, will need to deform to accommodate the thickness change of the membrane. This will lead to changes in contact resistance, the possibility of GDL 'tenting' into the flow channels and potentially irreversible damage to the GDL. This effect can be mitigated by avoiding dehydration of the membrane, introducing stress relief/constant compression mechanisms or designing the GDL to reversibly accommodate the requisite dimensional change.

Fig. 8 compares the resistance/displacement relationship obtained for the '*ex situ*' membrane and 'startup' MEA conditions. In order to compare both in terms of a relative displacement, the '*ex situ*' membrane thickness change was taken relative to that under ambient lab conditions (thickness of 178 μm). This is close to the initial resistance of the MEA prior to humidification ~835 mΩ cm^2.

Both have a common starting point in resistance and plateau in the region of ~200 mΩ cm^2 after an expansion of ~25 μm. The difference between the two trends can be attributed to the fact that that the 'ex situ' membrane is measured steady state and the 'startup' is dynamic. The CCU detects the maximum local sample expansion, while the resistance is a bulk measurement across the active area of the cell; therefore, heterogeneous swelling of the membrane will be detected as a full sample expansion (see how displacement leads resistance change in Fig. 7(a)), while the concomitant decrease in resistance associated with the expansion of a full membrane will not be measured. Localised electrical measurements have shown this to be the case [42].

Fig. 8 includes a line showing the minimum resistance measured for the MEA during flooding (discussed below). This shows that when the cell is operating, and electrolyte hydration has reached equilibrium, the resistance does equate to that of the *ex-situ* derived relationship.

3.3. Flooding effects on MEA operation

Durability studies of PEFC operation often feature abrupt 'spikes' of negative performance. These transients are usually the result of a flooding event at one of the electrodes (usually the cathode) [26]. Here we examine the effect on the membrane conductivity of these events and the impact on the dynamic stress/strain conditions in the cell.

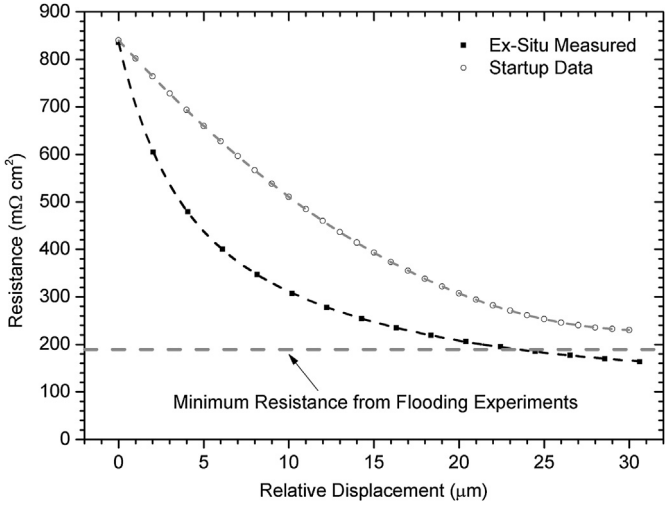

Fig. 8. Relationship between resistance and relative displacement, as calculated using Eq. (2) for an 'ex situ' membrane (steady state) and that observed for 'startup' (dynamic) under a controlled compression of 0.2 MPa.

Fig. 9 shows a cell running under non-ideal (over humidified) conditions, expected to lead to flooding. Large current spikes are observed over periods ranging up to 100 s, swelling of the membrane by over 30 μm and significant changes in the resistance of the membrane (over a range between 183 and 212 mΩ cm^2) are seen to be associated with the current spikes.

Fig. 10 shows the fuel cell operating in controlled displacement mode. The cell was operated at a constant voltage of 0.7 V with a flow rate of 50 ml min^{-1} for both the anode and cathode gas (H_2 and air). The controlled displacement mode enables the compression between the flow plates to be measured while the cell is running. Fig. 10 shows that resistance decreases when water flooding spikes occur, as seen previously, and the compression increases. The compression increase is due to the membrane swelling and forcing the GDL material into the flow field plate, which is detected by the CCU. The resistance is also measured with the range observed being greater than that observed in Fig. 9, this is due to the contact resistance change that occurs when the GDL material is compressed, as seen in Fig. 6. As the GDL is compressed into the flow field plate by the expanding electrolyte membrane there are several mechanisms that affect the overall ohmic response. The most significant of which are contact resistance change between the GDL material and the flow field plate and the increased internal connections between the fibres of the GDL [41].

3.4. Relationship between resistance, displacement and compression

Fig. 11 shows the relationship between the high frequency resistance and the thickness of the MEA (relative displacement) based on the time-varying data points for 'flooded mode' operation, similar to that in Fig. 9. The time-varying data points convert into a consistent relationship between resistance and thickness. As the membrane swells the resistance decreases to a point where the membrane has reached maximum saturation and the material's lowest resistance has been reached.

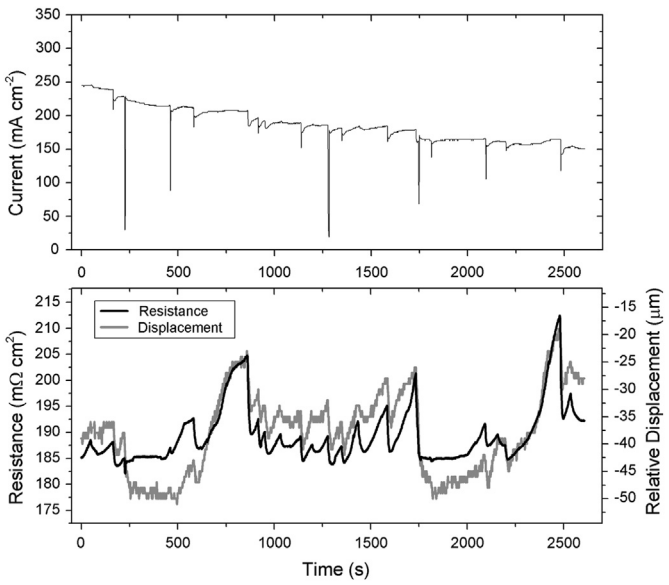

Fig. 9. Controlled compression mode (0.2 MPa): Voltage trace showing spikes in voltage caused by water flooding. The cell is run at high humidity resulting in the high frequency resistance decrease and subsequent increase in thickness observed. The cell was operated with constant voltage of 0.7 V at 80 °C with anode and cathode humidification of 100% RH at 85 °C and flow rates of 50 ml min^{-1} each. Displacement is relative to the thickness of the system at the start of the experiment (not shown).

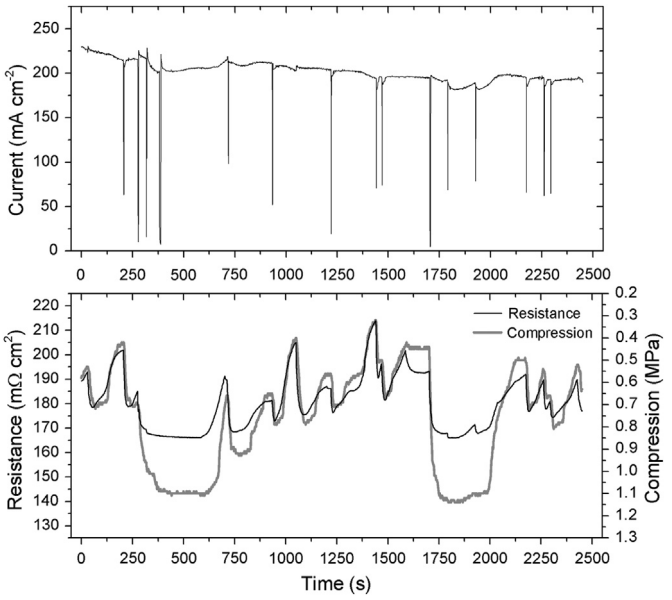

Fig. 10. Controlled displacement mode: Trends observed when displacement is held constant with the compression being measured while flooding spikes occur. The cell was operated with constant voltage of 0.7 V at 80 °C with anode and cathode humidification of 100% RH at 85 °C and flow rates of 50 ml min^{-1} each.

Fig. 12 shows the relationship between resistance and compression of an operating MEA in flooding mode, similar to that of Fig. 10. The lower resistance at the high compression region, compared to that in Fig. 11 at high displacement, is a result of the reduced GDL/contact resistance due to the 'crushing' effect of the expanding membrane on the GDL in constrained displacement mode.

At the fully compressed region (of Fig. 12) the resistance is approximately 15 mΩ cm^2 lower than for constant displacement operation (Fig. 11). Taking the value of the gradient of Fig. 6 as a guide to the reduction in resistance caused by GDL compression, it can be seen that this difference can be attributed to the crushing of the GDL, resulting in the previously reported improvement in bulk and contact resistance [41].

Figs. 11 and 12 are taken from an operating fuel cell undergoing flooding from liquid, water, whereas the startup relationship shown in Fig. 8 is for a dynamic process involving vapour phase water.

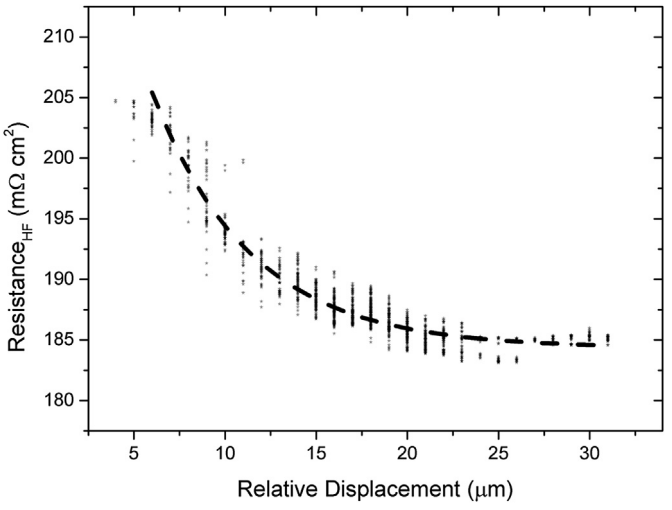

Fig. 11. Relationship between the resistance and the relative displacement of an operating MEA. The cell is operated in a 'flooding mode' similar to that of Fig. 9.

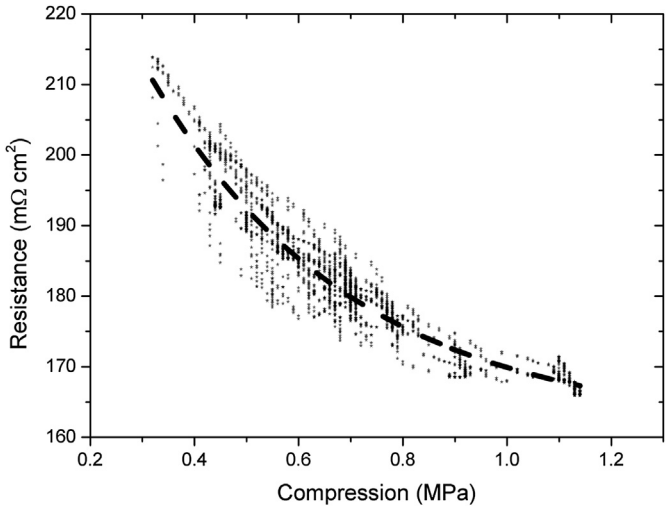

Fig. 12. Relationship between compression and resistance of an operating MEA that is constrained at a fixed displacement with a fit as a guide to the eye. The data is taken from a cell operating in flooding mode similar to Fig. 10.

Figs. 11 and 12 show that there is a consistent relationship between the resistance and mechanical properties, while Figs. 9 and 10 show that there is a correlation between the timing of current spikes (flooding events) and changes in resistance and dimension. However, there is no consistent quantitative relationship between the size of the current spike and the extent of the resistance/mechanical change. The reason for this is that the current spike is primarily a consequence of the blocking effect of water build-up in the cell, acting to starve the electrode of reactant. In a single channel serpentine flow field, liquid water removal is rapid and therefore the current spike is a relatively short lived event compared to liquid water induced membrane hydration. In addition, liquid water generation, as for example droplets in the flow field, is not a homogeneous process. Different amounts of the cell may be affected by the blocking and hydration effects.

Unlike the initial hydration process, in which each cell in a stack is likely to undergo the same process in unison and lead to an amplification of the expansion effect throughout a multi-cell stack, flooding events are more distributed in time and location. As such, the effect is not likely to have such a profound impact as initial hydration. However, flooding may lead to more localised membrane hydration which can cause heterogeneous membrane expansion which could have a mechanical 'twisting' effect on the cell or stack.

4. Conclusions

This study uses a commercially available cell compression unit that allows the dynamic relationship between membrane hydration, thickness and conductivity to be studied. Here, several operating modes of PEFCs are used, including start-up and flooding regimes, to observe the effects on the physical and electrochemical characteristics of the fuel cell.

During start-up of the fuel cell, significant compression changes occur (in controlled displacement mode) as the MEA hydrates, this type of hydration cycling will occur during repeated start-up and shutdown procedures and may lead to degradation in performance. The changes in membrane dimensions due to hydration transients that are translated through the GDL to result in a net change in thickness of the MEA (in controlled compression mode). In controlled displacement mode the overall thickness of the system

is constant and hence replicates a typical tie-bar type fuel cell construction, this leads to crushing of the GDL as it absorbs the increase in thickness (analogous to a spring) of the electrolyte, which in turn produces an increase in compression within the cell.

Flooding has a significant impact on the hydration state of the membrane as the liquid water is absorbed by the electrolyte that, in turn, affects the conductivity and causes a relatively large change in the thickness of the electrolyte.

Monitoring the change in thickness of the MEA during operation is a useful diagnostic to compliment conductivity and current/voltage measurement in determining the role of membrane hydration and contact resistance impact on fuel cell performance and durability. Flooding may be a major cause of long-term performance degradation due to the destructive nature of stress/strain cycles on the GDL caused by the hydration transients. The compression transients suggest that a dynamic compression control regime is beneficial for practical fuel cell construction.

Acknowledgements

The authors would like to acknowledge EPSRC Supergen Fuel Cells for supporting the work of Mason and Brett (EP/G030995/1) and the EPSRC 'Mind the Gap' UK/India project (EP/I037024/1) for supporting Millichamp and Brett.

References

[1] H. Li, Y. Tang, Z. Wang, Z. Shi, S. Wu, D. Song, J. Zhang, K. Fatih, J. Zhang, H. Wang, Z. Liu, R. Abouatallah, A. Mazza, J. Power Sources 178 (2008) 103–117.
[2] N. Yousfi-Steiner, P. Mocoteguy, D. Candusso, D. Hissel, A. Hernandez, A. Aslanides, J. Power Sources 183 (2008) 260–274.
[3] W. Dai, H. Wang, X.-Z. Yuan, J.J. Martin, D. Yang, J. Qiao, J. Ma, Int. J. Hydrogen Energ 34 (2009) 9461–9478.
[4] M. Eikerling, A.A. Kornyshev, A.R. Kucernak, Phys. Today 59 (2006) 38–44.
[5] T.A. Zawodzinski, J. Davey, J. Valerio, S. Gottesfeld, Electrochim. Acta 40 (1995) 297–302.
[6] T.A. Zawodzinski, C. Derouin, S. Radzinski, R.J. Sherman, V.T. Smith, T.E. Springer, S. Gottesfeld, J. Electrochem. Soc. 140 (1993) 1041–1047.
[7] T.E. Springer, T.A. Zawodzinski, S. Gottesfeld, J. Electrochem. Soc. 138 (1991) 2334–2342.
[8] E. Passalacqua, G. Squadrito, F. Lufrano, A. Patti, L. Giorgi, J. Appl. Electrochem. 31 (2001) 449–454.
[9] L.R. Jordan, A.K. Shukla, T. Behrsing, N.R. Avery, B.C. Muddle, M. Forsyth, J. Appl. Electrochem. 30 (2000) 641–646.
[10] S. Shimpalee, U. Beuscher, J.W. Van Zee, Electrochim. Acta 52 (2007) 6748–6754.
[11] C. Lim, C.Y. Wang, Electrochim. Acta 49 (2004) 4149–4156.
[12] H.K. Atiyeh, K. Karan, B. Peppley, A. Phoenix, E. Halliop, J. Pharoah, J. Power Sources 170 (2007) 111–121.
[13] S. Park, J.-W. Lee, B.N. Popov, J. Power Sources 163 (2006) 357–363.
[14] S. Park, B.N. Popov, Electrochim. Acta 54 (2009) 3473–3479.
[15] H.-S. Chu, C. Yeh, F. Chen, J. Power Sources 123 (2003) 1–9.
[16] X. Li, I. Sabir, J. Park, J. Power Sources 163 (2007) 933–942.
[17] X. Li, I. Sabir, Int. J. Hydrogen Energ 30 (2005) 359–371.
[18] J.r. Stumper, M. Lohr, S. Hamada, J. Power Sources 143 (2005) 150–157.
[19] M. Eikerling, A.A. Kornyshev, J. Electroanal. Chem. 475 (1999) 107–123.
[20] S. Ge, C.-Y. Wang, J. Electrochem. Soc. 154 (2007) B998–B1005.
[21] N. Holmström, J. Ihonen, A. Lundblad, G. Lindbergh, Fuel Cells 7 (2007) 306–313.
[22] D. Spernjak, A.K. Prasad, S.G. Advani, J. Power Sources 170 (2007) 334–344.
[23] A. El-kharouf, T.J. Mason, D.J.L. Brett, B.G. Pollet, J. Power Sources 218 (2012) 393–404.
[24] D.J.L. Brett, A.R. Kucernak, P. Aguiar, S.C. Atkins, N.P. Brandon, R. Clague, L.F. Cohen, G. Hinds, C. Kalyvas, G.J. Offer, B. Ladewig, R. Maher, A. Marquis, P. Shearing, N. Vasileiadis, V. Vesovic, ChemPhysChem 11 (2010) 2714–2731.
[25] J.-M. Le Canut, R.M. Abouatallah, D.A. Harrington, J. Electrochem. Soc. 153 (2006) A857–A864.
[26] F. Barbir, H. Gorgun, X. Wang, J. Power Sources 141 (2005) 96–101.
[27] D.J.L. Brett, S. Atkins, N.P. Brandon, N. Vasileiadis, V. Vesovic, A.R. Kucernak, J. Power Sources 172 (2007) 2–13.
[28] A. Hakenjos, H. Muenter, U. Wittstadt, C. Hebling, J. Power Sources 131 (2004) 213–216.
[29] K. Tuber, D. Pocza, C. Hebling, J. Power Sources 124 (2003) 403–414.
[30] F.Y. Zhang, X.G. Yang, C.Y. Wang, J. Electrochem. Soc. 153 (2006) A225–A232.
[31] X.G. Yang, F.Y. Zhang, A.L. Lubawy, C.Y. Wang, Electrochem. Solid St. 7 (2004) A408–A411.
[32] P.K. Sinha, P. Halleck, C.-Y. Wang, Electrochem. Solid St. 9 (2006) A344–A348.
[33] I. Manke, C. Hartnig, M. Grunerbel, W. Lehnert, N. Kardjilov, A. Haibel, A. Hilger, J. Banhart, H. Riesemeier, Appl. Phys. Lett. 90 (2007), 174105–174103.
[34] R. Satija, D.L. Jacobson, M. Arif, S.A. Werner, J. Power Sources 129 (2004) 238–245.
[35] N. Pekula, K. Heller, P.A. Chuang, A. Turhan, M.M. Mench, J.S. Brenizer, K. Unlu, Nucl. Instrum. Meth. A 542 (2005) 134–141.
[36] T.A. Trabold, J.P. Owejan, D.L. Jacobson, M. Arif, P.R. Huffman, Int. J. Heat Mass Trans. 49 (2006) 4712–4720.
[37] S. Tsushima, K. Teranishi, S. Hirai, Electrochem. Solid St. 7 (2004) A269–A272.
[38] K.W. Feindel, L.P.A. LaRocque, D. Starke, S.H. Bergens, R.E. Wasylishen, J. Am. Chem. Soc. 126 (2004) 11436–11437.
[39] M.H. Eikerling, K. Malek, in: David P. Wilkinson, Jiujun Zhang, Rob Hui, Jeffrey Fergus, X. Li (Eds.), Proton Exchange Membrane Fuel Cells: Materials Properties and Performance, CRC Press, 2010, pp. 343–435.
[40] M.B. Satterfield, P.W. Majsztrik, H. Ota, J.B. Benziger, A.B. Bocarsly, J. Polym. Sci. Pt B: Polym. Phys. 44 (2006) 2327–2345.
[41] T.J. Mason, J. Millichamp, T.P. Neville, A. El-kharouf, B.G. Pollet, D.J.L. Brett, J. Power Sources 219 (2012) 52–59.
[42] D.J. Brett, S. Atkins, N.P. Brandon, V. Vesovic, N. Vasileiadis, A. Kucernak, Electrochem. Solid-State Lett. 6 (2003) A63–A66.